Ceramics International 44 (2018) 23102–23108

Contents lists available at ScienceDirect

Ceramics International

journal homepage: www.elsevier.com/locate/ceramint

Effect of Mn doping on the chemical synthesis of interconnected nanoflakes-like CoS thin films for high performance supercapacitor applications

S.K. Shinde[a], M.B. Jalak[a], S.Y. Kim[a], H.M. Yadav[b], G.S. Ghodake[a], A.A. Kadam[c], D.-Y. Kim[a,*]

[a] Department of Biological and Environmental Science, Dongguk University-Ilsan, Biomedical Campus, Goyang-si, Gyeonggi-do 10326, Republic of Korea
[b] Department of Energy and Materials Engineering, Dongguk University, Seoul, Republic of Korea
[c] Research Institute of Biotechnology and Medical Converged Science, Dongguk University, Biomedi Campus, Ilsandong-gu, Goyang-si, Gyeonggi-do 10326, Republic of Korea

ARTICLE INFO

Keywords:
CoS thin films
Doping
XRD
Interconnected nanoflakes
Electrochemical testing

ABSTRACT

Herein, supercapacitor developed using Mn-doped CoS thin films (1–5% Mn) were prepared using the successive ionic layer adsorption and reaction (SILAR) method. The effect of the Mn-doped CoS thin films on the structural, morphological, and supercapacitor properties were studied using X-ray diffraction (XRD), X-ray photoelectron spectroscopy (XPS), field emission scanning electron microscopy (FE-SEM), transmission electron microscopy (TEM), and electrochemical evaluation. Doping up to 3% Mn lead to improvements in peak intensity. Also, the morphological results indicated that doping of Mn affected the CoS nanostructures. The 3% Mn-doped CoS electrodes had an interconnected nanoflakes-like nanostructure, with a high porosity compared to the other electrodes. XPS data strongly supported the XRD results. The Mn-doped CoS electrodes showed a higher capacitance (621 F g^{-1}) than the other electrodes, and electrochemical impedance spectroscopy indicated that the 3% Mn-doped CoS electrode was highly conductive. The characteristics of the 3% Mn-doped CoS electrode proved its applicability in supercapacitors.

1. Introduction

Recent years have experienced a substantial movement toward more, clean, environmental pollutant-free, low-cost, and sustainable energy sources. Several sustainable energy sources are available, like solar cells [1], batteries [2], fuel cells [3], oil, supercapacitors [4], and natural gas. Of these energy sources, solar cells, batteries, and supercapacitors are most favorable applicants for the energy conversion and storage [5–9], and all represent main energy sources for practical applications at the industry level in the portable electronic device industry [5,10–13]. Among these devices, supercapacitors are more beneficial, due to a high power density, long time charging-discharging [6–9], and long-term cyclic stability relative to conventional batteries [14–19]. Supercapacitors usually classified into different types: electrochemical double layer capacitors and pseudocapacitors [20].

Many researchers are currently working on the development of new nanostructures, such as hierarchical, hybrid, and hetero-structured nanomaterials, for improving the specific energy, power, and cycling stability [5,21]. Previously, different binary and ternary phases of cobalt sulfide/oxides, including several binary compounds, were investigated [22–26]. Recently, supercapacitors of ternary metal sulfides revealed as an exciting electrode material, due to its high redox reaction and high conductivity of $NiCo_2S_4$ electrodes [27].

Among the binary and ternary metal sulfide/semiconductors, binary CoS electrodes are the most capable electrode nanomaterials for supercapacitor application because of their high redox reaction, multiple and changeable valence states, as well as higher electrical conductivity. Hu et al. [3] successfully synthesized a hierarchical hollow nanostructure-like CoS electrode for electrochemical application, assembled from nanocubes, nanosheets (NSs), and nanoparticles (NPs) that resulted in double-shelled CoS-NP/CoS-NS constructs with exceptional capacitance (980 F g^{-1}) at current densities of 1 A g^{-1}. Faber et al. [24] prepared CoS_2 thin films by a thermal method on a glass substrate for solar cell applications and demonstrated that CoS_2 displayed high electrocatalytic activity in the electrolyte. Liu et al. [25] established a facile hydrothermal method to prepare a porous nanocoral-like Co_3S_4 thin film directly on a Ni foam. Both, the crystal growth mechanism and the development of the coral-like Co_3S_4 on Ni foam, were explained. Subsequent electrochemical testing revealed the Co_3S_4 electrode for supercapacitor has a large specific capacitance in KOH electrolyte. Xie et al. [28] used a hydrothermal approach to prepare carbon-coated CoS_2 as a thermal battery electrode, which presented higher cell

* Corresponding author.
E-mail address: sbpkim@dongguk.edu (D.-Y. Kim).

https://doi.org/10.1016/j.ceramint.2018.09.117
Received 2 August 2018; Received in revised form 11 September 2018; Accepted 12 September 2018
Available online 13 September 2018
0272-8842/ © 2018 Elsevier Ltd and Techna Group S.r.l. All rights reserved.

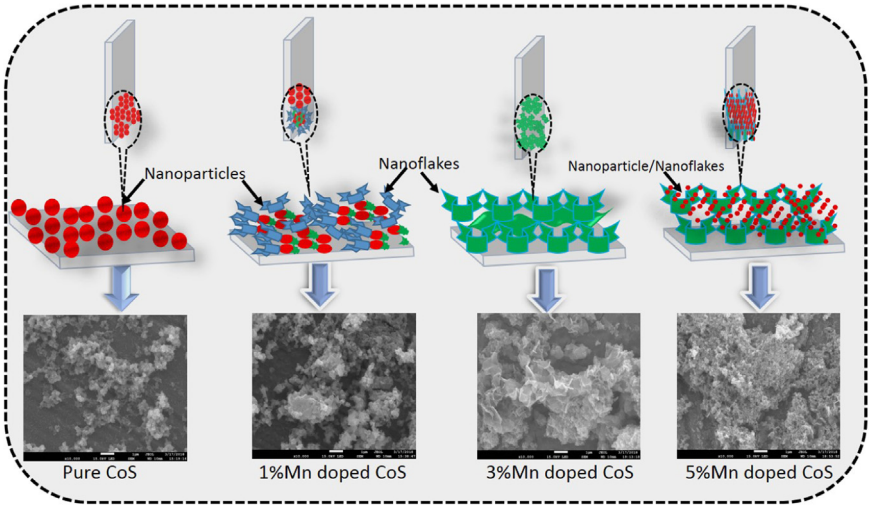

Fig. 1. Possible growth of the Mn-doped CoS thin films synthesized at different dopant percentages of Mn (1%, 3%, and 5%).

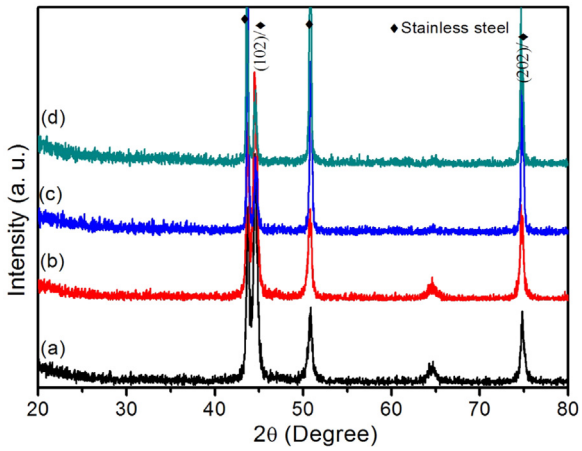

Fig. 2. XRD patterns of (a) as-syntheized CoS, (b) 1% Mn doped CoS, (b) 3% Mn doped CoS, (b) 5% Mn doped CoS thin films.

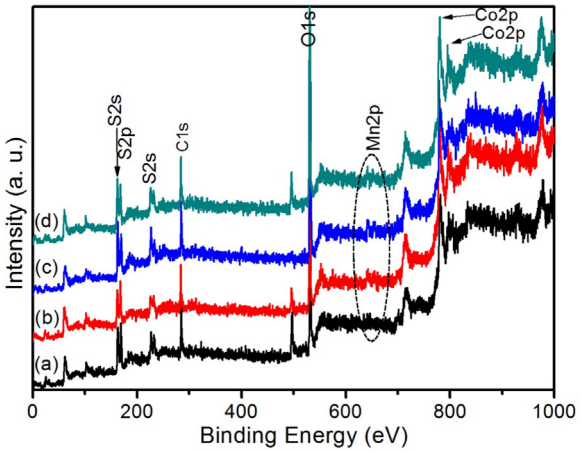

Fig. 3. Survey scan spectra of (a) as-syntheized CoS, (b) 1% Mn doped CoS, (b) 3% Mn doped CoS, (b) 5% Mn doped CoS thin films.

performance. CoS_2 hollow spheres [29] have been synthesized as nanostructured electrodes for supercapacitor application, using a facile solvothermal strategy. The as-prepared CoS_2 hollow spheres demonstrated extraordinary high discharge capacity and excellent cycling stability, signifying its potential as anode material for lithium-ion batteries.

In this paper, we report an innovative approach for the development of the hierarchical nanostructure of Mn-doped CoS thin films, for application as a supercapacitor electrode. The SILAR method successfully manufactured pure and various (1%, 3% and 5%) Mn-doped CoS electrodes. The structural, morphological, and supercapacitance of the CoS and Mn doping on the thin film using the X-ray diffraction, X-ray photoelectron spectroscopy, field emission scanning electron microscopy, transmission electron microscopy, cyclic voltammetry, galvanostatic charge/discharge, and electrochemical impedance spectroscopy, respectively. EIS results indicate that the 3% Mn-doped CoS electrode is more conductive than the other three electrodes, due to its lower value of the solution and charge-transfer resistance.

2. Experimental details

2.1. Materials

0.2 M $CoSO_4{\cdot}7H_2O$ (Cobalt (II) sulfate hydrate), 0.1 M $MnSO_4$ H_2O (Manganese sulfate monohydrate), 0.2 M Na_2S (Sodium sulfide), and NH_4OH (Ammonium hydroxide).

2.2. Synthesis of Mn-doped CoS samples

In a typical experiment, $CoSO_4$ and $MnSO_4$ sources were dissolved in double-distilled water (DDW), separately, and then combined at various ratios (e.g., 49:1, 47:3, and 45:5 mL of Co:Mn) to give final solution A (50 mL). We used double-distilled water for solutions B and D, for the losing bounding of Co^{2+}/Mn^{2+} and S^{2-} ions. The last solution was prepared by dissolving 1.68g Na_2S in 50 mL of DDW. Liquid ammonia (NH_3) was added to the combined solution of Co^{2+}/Mn^{2+} under constant magnetic stirring for 15 min. Later, preparation of all experimental solutions, as per solution A ($CoSO_4$ and $MnSO_4$) was used as a cationic precursor and solution C (Na2S) as an anionic precursor. Cleaned stainless-steel substrates were used as the working electrodes, which were dipped in solution A for 20 s, for deposition of Co^{2+}/Mn^{2+} ions. The Co^{2+}/Mn^{2+} coated stainless-steel substrate was then immersed in double-distilled water, for the losing bounding of Co^{2+}/Mn^{2+} ions. After washing away loosely bound ions, we used that sample for deposition of S on the Co^{2+}/Mn^{2+} -coated stainless-steel substrate. After completion of 10 cycles of deposition, the CoS-coated stainless-steel substrate was washed in double-distilled water and heated at 60 °C for 6 h. A similar procedure was used to prepare the 1%, 3%, and 5% Mn-doped CoS samples. Fig. 1 shows the growth of CoS and Mn-doped CoS thin films synthesized at different dopant (Mn)

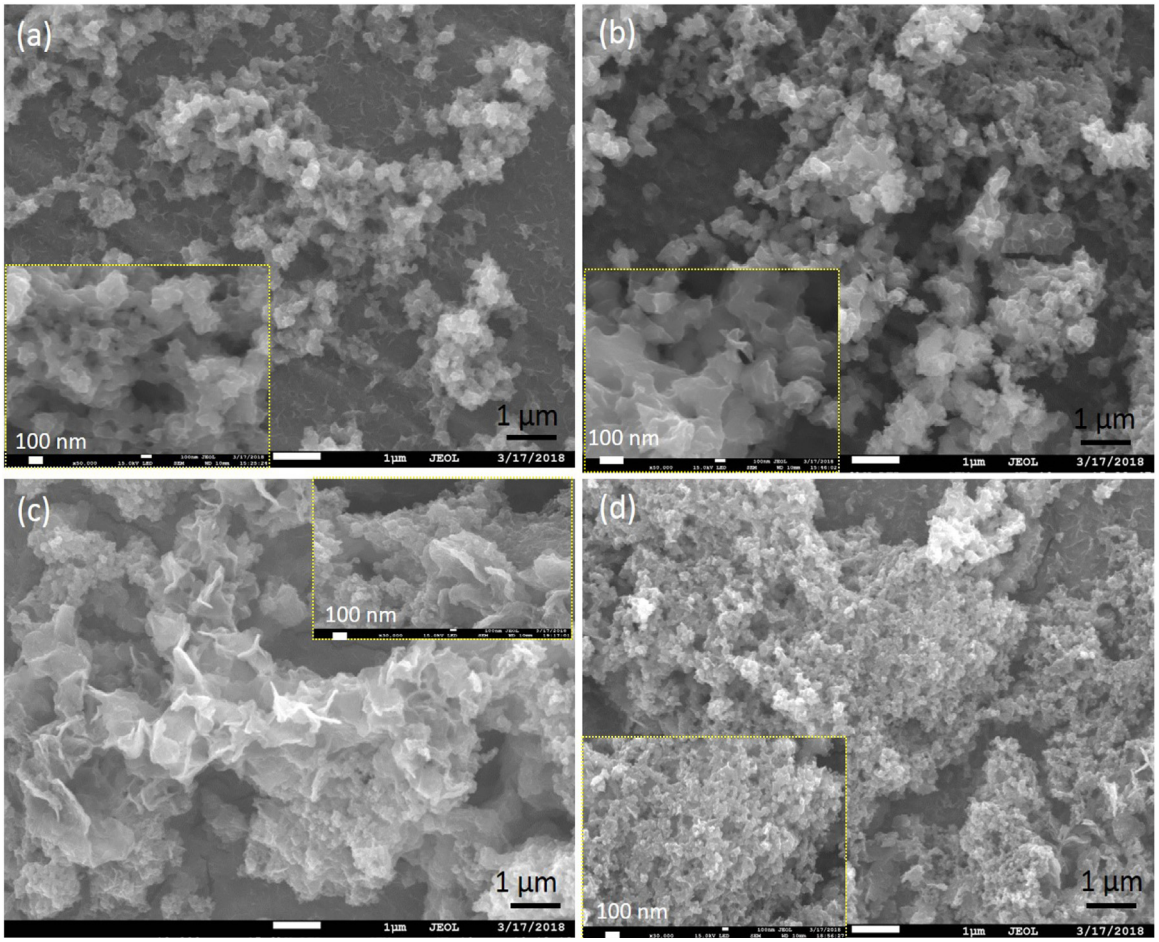

Fig. 4. FE-SEM microimage of the as-synthesized CoS, 1% Mn doped CoS, 3% Mn doped CoS, and 5% Mn doped CoS thin films, respectively, inset shows the high magnification images.

percentages. All prepared samples were evaluated by structural, morphological, and electrochemical testing.

The crystal structure of all prepared pure and Mn-doped CoS thin films were characterized by XRD (Rigaku D/Max-KA), using Cu K_α radiation. X-ray photoelectron spectroscopy (XPS; ULVAC-PHI Quantera SXM) and an FE-SEM instrument (Hitachi, Model SU-70) was used to examine the surface morphology and nanostructures of the as-synthesized pure CoS and Mn-doped CoS thin films. The nanostructures of the prepared pure CoS and Mn-doped CoS samples were studied by TEM method (Jeol, Model JEM-2100) [30].

2.3. Electrochemical testing

The supercapacitor properties of the Mn doped CoS electrodes were tested using an as-synthesized pure and Mn doped CoS samples as a working electrode, which was synthesized at different doping percentage of Mn [31]. A three-electrode cell was used, which included a pure and Mn doped CoS electrode as the working electrode, Pt as the counter electrode, and Ag/AgCl electrode as the reference electrode. The reference electrode was connected to an Ag/AgCl electrode, and the counter electrode probe was connected to a thin Pt electrode. The working electrode probe connected to the Mn doped CoS electrode was immersed in 3 M KOH electrolyte solution. The supercapacitor properties were tested in the potential window −0.2–0.6 V. EIS examinations were completed by applying an excitation voltage of 5 mV to the cells, and the frequency range was from 0.01 to 100 kHz [32]. In supercapacitor measurements, cyclic voltammetry (CV), galvanostatic charge/discharge, and electrochemical impedance spectroscopy (EIS) measurements were performed with a CHI 660E electrochemical workstation in aqueous 3 M KOH electrolyte [27,31,33]. Specific capacitances were calculated from the CV and galvanostatic discharge curves, using the following relation, respectively:

$$Cs = I\Delta t/(m\Delta V) \quad (1)$$

$$C_s = \frac{\int IdV}{mv\Delta V} \quad (2)$$

where, C_s is the specific capacitance, I is the discharge time, Δt is the discharge time, ΔV is the voltage range, and m is the mass of the active materials of the electrode.

3. Results and discussion

3.1. X-ray diffraction (XRD) analysis

The XRD characterization technique allowed confirming the phase and crystal structure of the as-synthesized and Mn-doped CoS samples. The pure and Mn-doped CoS samples were synthesized using the SILAR method at constant SILAR cycle, for the supercapacitor application. Fig. 2 displays the XRD patterns of pure CoS thin films and those doped with Mn (1%, 3%, and 5%), using SILAR cycles. The XRD patterns of the Mn-doped CoS thin films are typical of CoS materials [32,33]. The CoS thin films show peaks at 44.44° and 74.50°, which can be assigned to the (102) and (202) planes of hexagonal CoS, and all peaks agree with the literature data (JCPDS card number 65-3418) [34]. After doping the CoS thin films with Mn, there is no change in the peak angles, only peak intensity. The 3% Mn-doped CoS thin films reveal peaks of higher

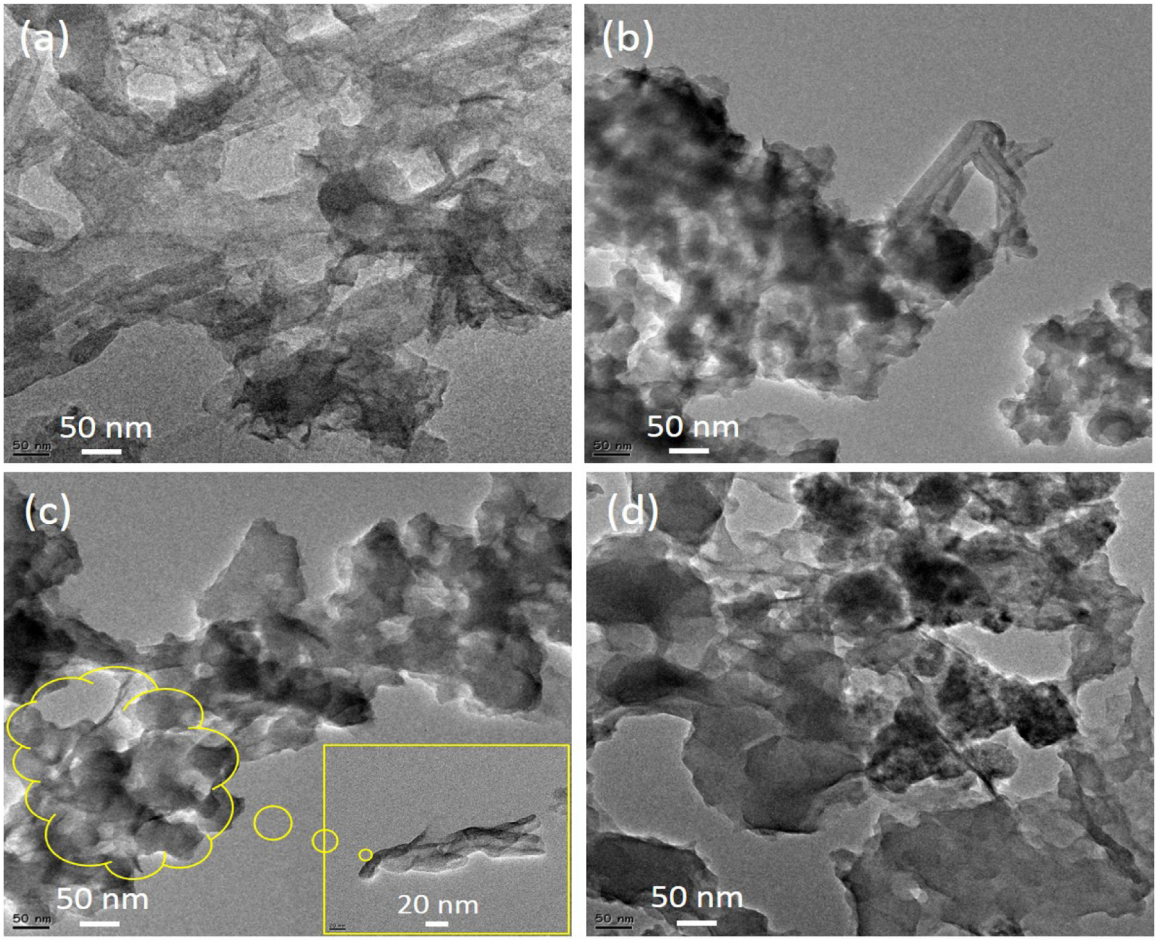

Fig. 5. TEM images of (a) as-synthesized CoS, (b) 1% Mn doped CoS, (b) 3% Mn doped CoS, (b) 5% Mn doped CoS thin films.

intensity, suggesting that this sample has higher crystallinity and is potentially better electronic conductivity relative to the pure CoS sample and other Mn-doped samples [25,34].

3.2. X-ray photoelectron spectroscopy (XPS) analysis

XPS analysis was undertaken for further phase, chemical, and elemental state identification of pure CoS and Mn:CoS samples. Fig. 3 shows the survey spectrum of pure CoS and Mn-doped CoS thin films. The pure CoS thin films demonstrated binding energies of 162.68 eV, 531.82 eV, 654.15 eV, and 780.63 eV, corresponding to S 2p, O 1s, Mn 2p, and Co 2p, respectively [25]. The results indicate that all elements are present in the as-prepared and Mn-doped samples. The intense peaks at 780.63 eV and 795.97 eV (Fig. 3a–d) well-fit to the Co $2p_{1/2}$ and Co $2p_{3/2}$ spin-orbits doublets of Co^{2+} and Co^{3+}, respectively [32]. We observed greater intensity in the peaks after adding dopant (Mn) to the CoS thin films as compared to the pure CoS samples. Also, the peak at 531.82 eV has a higher intensity than those corresponding to the Co^{2+} and Mn^{2+} elements, which specifies the existence of more adsorbed O1s elements on the surface of pure CoS and Mn-doped thin films [35]. The binding energies at 160.68 eV and 168.98 eV concur with the S $2p_{3/2}$ and S $2p_{1/2}$ energy levels of CoS thin films. Hence, the XPS analysis confirmed the phase formation of CoS thin films, as reported previously [25,35,36].

3.3. Field emission scanning electron microscopy (FE-SEM) analysis

FE-SEM provided detailed information regarding the surface morphology of the CoS and Mn-doped thin films. Fig. 4 displays the FE-SEM micro images of the pure CoS and Mn-doped thin films, at various magnifications, synthesized using the SILAR method. The micrograph of the pure CoS sample (Fig. 4a) illustrates the growing stage of vertical interconnected nanoflakes-like nanostructures on the stainless-steel substrate, but the sample is not fully covered, indicating poor or insufficient growth of Co and S elements on the stainless-steel [37]. After Mn doping, the thin films are fully covered with diverse nanostructures of interconnected NPs, interconnected nanoflakes (NFs), and NPs covering NFs. Fig. 4b and c shows the FE-SEM micrograph of 1% Mn-doped thin films, as the NP start to aggregate and convert to the porous NFs-like nanostructure. Interconnected chain of vertical nanoflakes-like nanostructures can be seen growing on the stainless-steel substrate in the 3% Mn-doped thin films. The size and thickness of the individual nanoflake is much smaller than the other nanostructures, suggesting the 3% Mn-doped film is suitable for the electrochemical reaction because this type of surface morphology provides the maximum surface area of the sample. Further increasing the Mn dopant percentage to 5% Mn leads to the overgrowth of the nanostructure (Fig. 4d), which is not applicable for the supercapacitor application as compared to the 3% Mn [37–39].

3.4. Transmission electron microscopy (TEM) analysis

TEM analysis was performed to gain more insight into the surface morphology of the as-synthesized pure and Mn-doped thin films, which, as mentioned above, were fabricated using the SILAR method, for supercapacitor application. Visualization of the pure CoS thin film (Fig. 5a) reveals an average length of nanosheets of 110–125 nm, and a porous surface, consistent with the FE-SEM images [40]. Fig. 5b–d

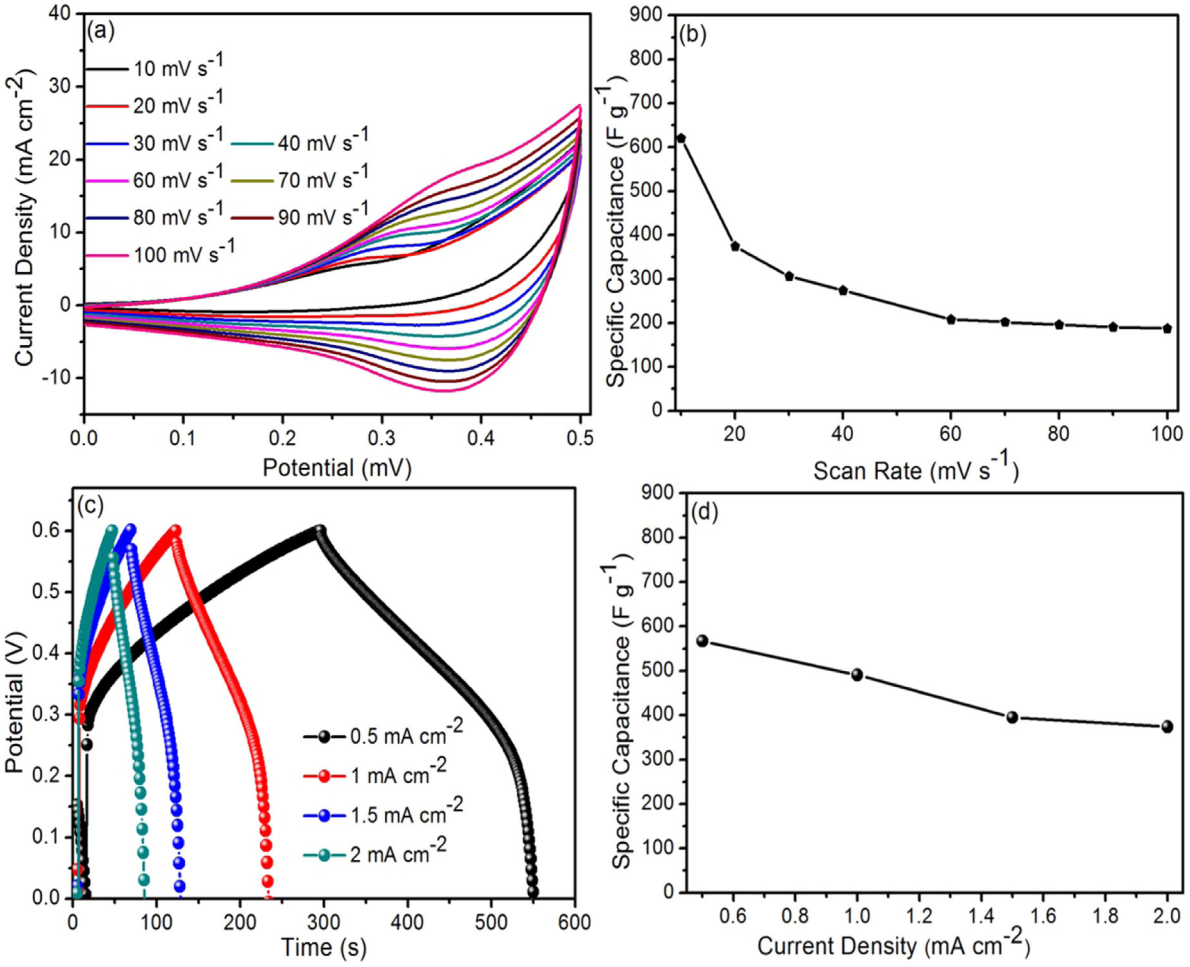

Fig. 6. (a) CV curves of 3% Mn doped CoS thin films at different scan rates from 10 to 100 mV s^{-1} respectively, (b) Specific capacitance of 3%Mn:CoS electrode at different scan rates from 10 m to 100 mV s^{-1}, (c) Galvanostatic charge-discharge of 3% Mn:CoS electrode at different current densities from 0.5 to 2 mA cm^{-2}, (d) Specific capacitance of 3% Mn doped CoS electrode at different current densities.

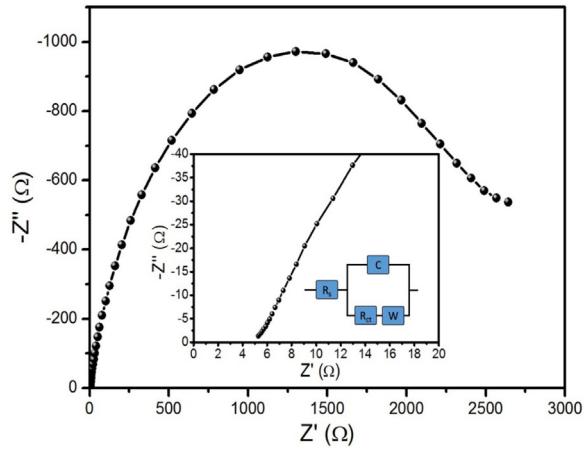

Fig. 7. Nyquist plot of 3% Mn doped CoS electrode.

shows the TEM images of 1%, 3%, and 5% Mn-doped thin films, respectively. At 3% Mn dopant (Fig. 5c), a highly porous nanostructure is evident, indicating that it provides a higher reactive surface area as compared to the other electrodes [32,33], which is more useful for electrochemical testing for the supercapacitor application. Therefore, we concluded the 3% Mn-doped CoS_2 electrode is the most suitable for the measurement of the electrochemical and supercapacitor properties [1,32,33]. All images obtained by TEM corroborated those obtained by FE-SEM.

3.5. Electrochemical testing

The supercapacitor properties of the pure CoS, and 1%, 3%, and 5% Mn-doped electrodes were individually evaluated using the CV technique at 100 mV s^{-1} scan rate. Fig. S1a shows the CV curves at 100 mV s^{-1} scan rate, for pure CoS and 1%, 3%, and 5% Mn-doped CoS electrodes, respectively, in the 0.0–0.5 V range. It is seen that the doping percentages affect both redox peaks of the CoS electrodes [41]. The active deposited mass of pure CoS and 1%, 3%, and 5% Mn-doped CoS electrodes at constant SILAR cycles, was found to be 0.27, 0.29, and 0.23, 0.20 mg cm^{-2}, respectively. The 3% Mn-doped CoS electrode displayed higher current density, which is proportional to the specific capacitance of the sample. At 100 mV s^{-1} scan rate, the specific capacitance is 288 F g^{-1} for pure CoS, and 347, 621, and 433 F g^{-1} for 1%, 3%, and 5% Mn-doped CoS electrodes, respectively (Fig. S1b). The evaluated results prove that the 3% Mn-doped CoS electrode is a superior electrode material with high capacitance because this composition resulted in a comparatively higher surface area. Fig. 6a shows the CV curves (scan rate range of 10–100 mV s^{-1}) of 3% Mn-doped electrodes in 3 M KOH electrolyte. When tested in the range 0.0–0.5 V, the 3% Mn-doped CoS has superior capacitance compared to pure CoS, 1% Mn, and 5% Mn [42]. The resultant scan rates increase as the scan rate increases, demonstrating 3% Mn-doped electrodes have good capacitive nature, which is attributed to the high areal active surfaces of the three-

dimensional interconnected NFs of the 3% Mn-doped electrode and easy transfer of ions from the very thin NFs to the counter electrode [22]. At the scan rate range of 10–100 mV s^{-1}, 3% Mn-doped CoS electrode possesses a specific capacitance of 621 F g^{-1} at 10 mV s^{-1} (Fig. 6b). The galvanostatic charge/discharge study was conducted at different current densities (0.5–2.0 mA cm^{-2}), to supplement calculation of the specific capacitance of the 3% Mn-doped CoS electrode. As evident in Fig. 6c, the galvanostatic charge/discharge curves indicate 3% Mn-doped electrode has a good charging/discharging capacity [41,43]. The calculated value of specific capacitance is 566 F g^{-1} at a current density of 0.5 mA cm^{-2} (Fig. 6d), which is similar to that reported in the literature [42,43]. EIS measurements have been used to identify the electrochemical behaviors of the 3% Mn-doped CoS electrode in 3 M KOH electrolyte. Fig. 7 displays the Nyquist plot of the 3% Mn-doped electrodes, highlighting a very low charge transfer resistance and solution resistance, which indicates that the electrode shows a rapid ion exchange process, due to the interconnected nanostructure that provided a highly effective reactive surface [31,42–44].

4. Conclusions

We deposited Mn-doped CoS thin films on a stainless-steel substrate, for supercapacitor application, by using an easy and low-cost SILAR method. The typical nanostructure provides many advantages of Mn-doped CoS electrodes, such as a high surface area, porous surface, low solution resistance, and short diffusion path of ions. After measurements of the supercapacitor properties, the 3% Mn-doped CoS electrode shows superior performance with a specific capacitance of 621 F g^{-1} at 10 mV s^{-1}, in 3 M KOH electrolyte. The calculated specific capacitance is almost two times higher than the pure CoS and the other Mn-doped electrodes, indicating that doping of Mn affects the supercapacitor performance. Based on the results, the 3% Mn-doped CoS electrode is a promising composition for high supercapacitor application, and the SILAR method enables the design of new nanostructures for other transition metal oxide/sulfides.

Acknowledgements

This work was supported by the Dongguk University Research Fund of 2018.

Appendix A. Supplementary material

Supplementary data associated with this article can be found in the online version at doi:10.1016/j.ceramint.2018.09.117.

References

[1] P. Hasin, Electrochemical milling process to synthesize amorphous CoS as efficient electrocatalyst for the counter electrode of an efficient dye-sensitized solar cell, Sol. Energy 135 (2016) 398–407.
[2] D. Dubal, P. Gomez-Romero, Metal Oxides in Supercapacitors, ISBN: 9780128104651.
[3] H. Hu, B.Y. Guan, X.W. Lou, Construction of complex CoS hollow structures with enhanced electrochemical properties for hybrid supercapacitors, Chem (2016) 102–113.
[4] D.P. Dubal, O. Ayyad, V. Ruiz, P. Gómez-Romero, Hybrid energy storage: the merging of battery and supercapacitor chemistries, Chem. Soc. Rev. 44 (2015) 1777–1790.
[5] J.-C. Xing, Y.-L. Zhu, Q.-W. Zhou, X.-D. Zheng, Q.-J. Jiao, Fabrication and shape evolution of CoS2 octahedrons for application in supercapacitors, Electrochim. Acta 136 (2014) 550–556.
[6] Y. Chen, B. Qu, L. Hu, Z. Xu, Q. Li, T. Wang, High-performance supercapacitor and lithium-ion battery based on 3D hierarchical NH_4F-induced nickel cobaltate nanosheet–nanowire cluster arrays as self-supported electrodes, Nanoscale 5 (2013) 9812–9820.
[7] P. Simon, Y. Gogotsi, Materials for electrochemical capacitors, Nat. Mater. 7 (2008) 845–854.
[8] S. Peng, L. Li, H. Tan, R. Cai, W. Shi, C. Li, S.G. Mhaisalkar, M. Srinivasan, S. Ramakrishna, Q. Yan, MS2 (M = Co and Ni) hollow spheres with tunable interiors for high-performance supercapacitors and photovoltaics, Adv. Funct. Mater. 24 (2014) 2155–2162.
[9] M. Winter, R.J. Brodd, What are batteries, fuel cells, and supercapacitors? Chem. Rev. 104 (2004) 4245–4270.
[10] M. Zhi, C. Xiang, J. Li, M. Li, N. Wu, Nanostructured carbon–metal oxide composite electrodes for supercapacitors: a review, Nanoscale 5 (2013) 72–88.
[11] S.K. Shinde, D.P. Dubal, G.S. Ghodake, D.-Y. Kim, V.J. Fulari, Morphological tuning of CuO nanostructures by simple preparative parameters in SILAR method and their consequent effect on supercapacitors, Nano-Struct. Nano-Objects 6 (2016) 5–13.
[12] Y.-G. Guo, J.-S. Hu, L.-J. Wan, Nanostructured materials for electrochemical energy conversion and storage devices, Adv. Mater. 20 (2008) 2878–2887.
[13] B. Dunn, H. Kamath, J.-M. Tarascon, Electrical energy storage for the grid: a battery of choices, Science 334 (2011) 928–935.
[14] W. Chen, C. Xia, H.N. Alshareef, One-step electrodeposited nickel cobalt sulfide nanosheet arrays for high-performance asymmetric supercapacitors, ACS Nano 8 (2014) 9531–9541.
[15] H. Pang, C. Wei, X. Li, G. Li, Y. Ma, S. Li, J. Chen, J. Zhang, Microwave-assisted synthesis of NiS2 nanostructures for supercapacitors and cocatalytic enhancing photocatalytic H2 production, Sci. Rep. 4 (2014) 3577–3585.
[16] J. Jiang, Y. Li, J. Liu, X. Huang, C. Yuan, X.W. Lou, Recent advances in metal oxide-based electrode architecture design for electrochemical energy storage, Adv. Mater. 24 (2012) 5166–5180.
[17] M.-R. Gao, Y.-F. Xu, J. Jiang, S.-H. Yu, Nanostructured metal chalcogenides: synthesis, modification, and applications in energy conversion and storage devices, Chem. Soc. Rev. 42 (2013) 2986–3017.
[18] Q. Wang, Y. Zhu, J. Xue, X. Zhao, Z. Guo, C. Wang, General synthesis of porous mixed metal oxide hollow spheres with enhanced supercapacitive properties, ACS Appl. Mater. Interfaces 8 (2016) 17226–17232.
[19] H.B. Wu, H. Pang, X.W. Lou, Facile synthesis of mesoporous Ni0.3Co2.7O4 hierarchical structures for high-performance supercapacitors, Energy Environ. Sci. 6 (2013) 3619–3626.
[20] L. Jinlong, L. Tongxiang, Y. Meng, K. Suzuki, H. Miura, Comparing different microstructures of CoS formed on bare Ni foam and Ni foam coated graphene and their supercapacitors performance, Colloids Surf. A: Physicochem. Eng. Asp. 529 (2017) 57–63.
[21] L.-Q. Mai, F. Yang, Y.-L. Zhao, X. Xu, L. Xu, Y.-Z. Luo, Hierarchical MnMoO4/CoMoO4 heterostructured nanowires with enhanced supercapacitor performance, Nat. Commun. 2 (2011) 381.
[22] H. Chen, X. Zhu, Y. Chang, J. Cai, R. Zhao, 3D flower-like CoS hierarchitectures recycled from spent LiCoO2 batteries and its application in electrochemical capacitor, Mater. Lett. 218 (2018) 40–43.
[23] X. Zeng, B. Yang, X. Li, R. Yu, Three-dimensional hollow CoS2 nanoframes fabricated by anion replacement and their enhanced pseudocapacitive performances, Electrochim. Acta 240 (2017) 341–349.
[24] M.S. Faber, K. Park, M. Cabán-Acevedo, P.K. Santra, S. Jin, Earth-abundant cobalt pyrite (CoS2) thin film on glass as a robust, high-performance counter electrode for quantum dot-sensitized solar cells, J. Phys. Chem. Lett. 4 (2013) 1843–1849.
[25] G. Liu, B. Wang, L. Wang, T. Liu, T. Gao, D. Wang, Facile controlled synthesis of a hierarchical porous nanocoral-like Co3S4 electrode for high-performance supercapacitors, RSC Adv. 6 (2016) 54076–54086.
[26] L. Zhang, Y. Wang, W. Zhou, G. Song, S. Cheng, Facile synthesis of hollow Co9S8 nanospheres for high performance pseudocapacitor, Int. J. Electrochem. Sci. 11 (2016) 1541–1548.
[27] D.-Y. Kim, G.S. Ghodake, N.C. Maile, A.A. Kadam, D.S. Lee, V.J. Fulari, S.K. Shinde, Chemical synthesis of hierarchical NiCo2S4 nanosheets like nanostructure on flexible foil for a high performance supercapacitor, Sci. Rep. 7 (2017) 9764–9774.
[28] S. Xie, Y. Deng, J. Mei, Z. Yang, W.-M. Lau, H. Liu, Carbon coated CoS2 thermal battery electrode material with enhanced discharge performances and air stability, Electrochim. Acta 231 (2017) 287–293.
[29] Q. Wang, L. Jiao, Y. Han, H. Du, W. Peng, Q. Huan, D. Song, Y. Si, Y. Wang, H. Yuan, CoS2 hollow spheres: fabrication and their application in lithium-ion batteries, J. Phys. Chem. C 115 (2011) 8300–8304.
[30] Z. Zhang, Q. Li, Z. Li, J. Ma, C. Li, L. Yin, X. Gao, Partially reducing reaction tailored mesoporous 3D carbon coated NiCo-NiCoO2/carbon xerogel hybrids as anode materials for lithium ion battery with enhanced electrochemical performance, Electrochim. Acta 203 (2016) 117–127.
[31] S.K. Shinde, D.P. Dubal, G.S. Ghodake, D.Y. Kim, V.J. Fulari, Nanoflower-like CuO/$Cu(OH)_2$ hybrid thin films: synthesis and electrochemical supercapacitive properties, J. Electroanal. Chem. 732 (2014) 80–85.
[32] W. Zeng, G. Zhang, X. Wu, K. Zhang, H. Zhang, S. Hou, C. Li, T. Wang, H. Duan, Construction of hierarchical CoS nanowire@$NiCo_2S_4$ nanosheet arrays via one-step ion exchange for high-performance supercapacitors, J. Mater. Chem. A 3 (2015) 24033–24040.
[33] S.K. Shinde, D.P. Dubal, G.S. Ghodake, V.J. Fulari, Hierarchical 3D-flower-like CuO nanostructure on copper foil for supercapacitors, RSC Adv. 5 (2015) 4443–4447.
[34] C.V.V.M. Gopi, S. Ravi, S.S. Rao, A.E. Reddy, H.-J. Kim, Carbon nanotube/metal-sulfide composite flexible electrodes for high-performance quantum dot-sensitized solar cells and supercapacitors, Sci. Rep. 7 (2017) 46519–46531.
[35] H.-J. Kim, H.-D. Lee, S.S. Rao, A.E. Reddy, S.-K. Kim, C.V. Thulasi-Varma, Well-dispersed NiS nanoparticles grown on a functionalized CoS nanosphere surface as a high performance counter electrode for quantum dot sensitized solar cells, RSC Adv. 6 (2016) 29003–29019.
[36] R. Gao, Q. Zhang, F. Soyekwo, C. Lin, R. Lv, Y. Qu, M. Chen, A. Zhu, Q. Liu, Novel amorphous nickel sulfide@CoS double-shelled polyhedral nanocages for supercapacitor electrode materials with superior electrochemical properties, Electrochim. Acta 237 (2017) 94–101.
[37] S.K. Shinde, V.J. Fulari, D.-Y. Kim, N.C. Maile, R.R. Koli, H.D. Dhaygude,

G.S. Ghodake, Chemical synthesis of flower-like hybrid Cu(OH)2/CuO electrode: application of polyvinyl alcohol and Triton X−100 to enhance supercapacitor performance, Colloids Surf. B: Biointerfaces 156 (2017) 165–174.
[38] S.K. Shinde, D.-Y. Kim, G.S. Ghodake, N.C. Maile, A.A. Kadam, D.S. Lee, M.C. Rath, V.J. Fulari, Morphological enhancement to CuO nanostructures by electron beam irradiation for biocompatibility and electrochemical performance, Ultrason. Sonochem. 40 (2018) 314–322.
[39] S.K. Shinde, G.S. Ghodake, D.P. Dubal, G.M. Lohar, D.S. Lee, V.J. Fulari, Structural, optical, and photo-electrochemical properties of marygold-like CdSe0.6Te0.4 synthesized by electrochemical route, Ceram. Int. 40 (2014) 11519–11524.
[40] T. Xiao, J. Li, X. Zhang, W. Zhang, S. Wang, X. Chen, P. Xiang, L. Jiang, X. Tan, Wide potential window and high specific capacitance triggered via rough NiCo2S4 nanorod arrays with open top for symmetric supercapacitors, Electrochim. Acta 269 (2018) 397–404.
[41] C. Su, J. Xiang, F. Wen, L. Song, C. Mu, D. Xu, C. Hao, Z. Liu, Microwave synthesized three-dimensional hierarchical nanostructure CoS2/MoS2 growth on carbon fiber cloth: a bifunctional electrode for hydrogen evolution reaction and supercapacitor, Electrochim. Acta 212 (2016) 941–949.
[42] J.-C. Xing, Y.-L. Zhu, M.-Y. Li, Q.-J. Jiao, Hierarchical mesoporous CoS2 microspheres: morphology-controlled synthesis and their superior pseudocapacitive properties, Electrochim. Acta 149 (2014) 285–292.
[43] S. Chen, Y. Yang, Z. Zhan, J. Xie, J. Xiong, Designed construction of hierarchical NiCo2S4@polypyrrole core–shell nanosheet arrays as electrode materials for high-performance hybrid supercapacitors, RSC Adv. 7 (2017) 18447–18455.
[44] S.K. Shinde, D.P. Dubal, G.S. Ghodake, P. GomezRomero, S. Kim, V.J. Fulari, Influence of Mn incorporation on the supercapacitive properties of hybrid CuO/Cu(OH)2 electrodes, RSC Adv. 5 (2015) 30478–30484.